

Bridging the gap between paired and unpaired medical image translation

Pauliina Paavilainen^{1,2}, Saad Ullah Akram^{1,2}[0000-0002-2570-5870], and Juho Kannala¹[0000-0001-5088-4041]

¹ Aalto University, Finland

² MVision AI, Finland

{pauliina.paavilainen, saad.akram}@mvision.ai

Abstract. Medical image translation has the potential to reduce the imaging workload, by removing the need to capture some sequences, and to reduce the annotation burden for developing machine learning methods. GANs have been used successfully to translate images from one domain to another, such as MR to CT. At present, paired data (registered MR and CT images) or extra supervision (e.g. segmentation masks) is needed to learn good translation models. Registering multiple modalities or annotating structures within each of them is a tedious and laborious task. Thus, there is a need to develop improved translation methods for unpaired data. Here, we introduce modified pix2pix models for tasks CT→MR and MR→CT, trained with unpaired CT and MR data, and MRCAT pairs generated from the MR scans. The proposed modifications utilize the paired MR and MRCAT images to ensure good alignment between input and translated images, and unpaired CT images ensure the MR→CT model produces realistic-looking CT and CT→MR model works well with real CT as input. The proposed pix2pix variants outperform baseline pix2pix, pix2pixHD and CycleGAN in terms of FID and KID, and generate more realistic looking CT and MR translations.

Keywords: Medical image translation · Generative adversarial network

1 Introduction

Each medical imaging modality captures specific characteristics of the patient. In many medical applications, complimentary information from multiple modalities can be combined for better diagnosis or treatment. However, due to limited time, cost and patient safety, not all desired modalities are captured for every patient. Medical image translation can play a vital role in many of these scenarios as it can be used to generate non-critical (i.e. the ones which are not needed for fine pattern matching) missing modalities. One such clinical application is in MR-based radiotherapy, where MR images are used for delineating targets (e.g. tumors) and organs-at-risk (OARs). However, the clinicians still need CT scans for calculating the dose delivered to OARs and targets. Since this CT scan is used to compute dose delivered to various structures, the alignment of the patient

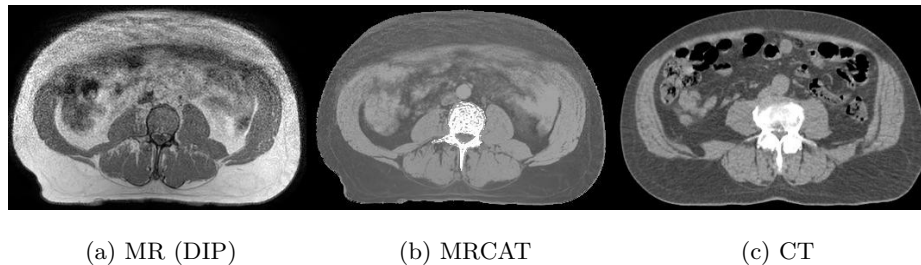


Fig. 1: MR and MRCAT are voxel-aligned, while CT is from a different patient.

anatomy is more important than the precise voxel intensities. There exist few commercial solutions which can be used to generate synthetic CT scans, such as Philips’ MRCAT. However, these translated images do not look very realistic due to quantization artifacts, failure to reduce blurring caused by patient breathing and lack of air cavities, etc. (see Fig. 1b).

Medical image translation can also play a critical role in development of machine learning based image analysis methods. In many applications, same tasks are performed in different modalities, e.g. in radiotherapy, OAR contouring is done in either CT or MR. Medical image translation can significantly speed-up the development of these automated methods by reducing the annotation requirements for new modalities/sequences. A large dataset can be annotated in one modality and then image translation can be used to generate scans of new modalities and annotations copied to synthetic scans.

During recent years, there has been increased interest in using Generative Adversarial Networks (GANs) [8] in medical image generation. The research in the field includes low-dose CT denoising [28], MR to CT translation [19,27,7,20], CT to MR translation [13], applications in deformable image registration [24] and segmentation [12], data augmentation [23], PET to CT translation, MR motion correction [1], and PET denoising [2] (for review, see [29]).

pix2pix [11] and CycleGAN [32] are two popular general-purpose image-to-image translation methods. pix2pix requires paired and registered data, while CycleGAN can be trained with unpaired images. pix2pix and its variants can produce high quality realistic-looking translations, however, capturing voxel-aligned scans or registering scans is a time-consuming task. In the medical imaging field, there is often lack of paired data, making CycleGAN more suitable method. However, without any additional constraints, it is difficult to optimize and the translated images may not always have good alignment with input scans. Many variants have been proposed which impose additional constraints, e.g. mask alignment between both input and output scans [31].

Besides CycleGAN, another relatively popular unpaired image-to-image translation method is UNsupervised Image-to-image Translation (UNIT) [18], which is a Variational Autoencoder (VAE)-GAN-based method [15,8,16]. UNIT has been utilized for T1 to T2 MR and T2 to T1 MR translation [26], PET to CT

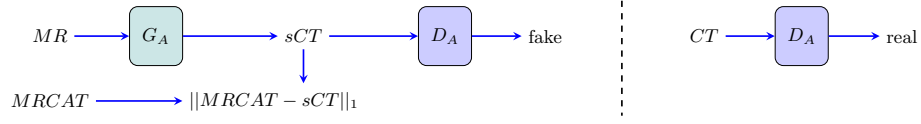


Fig. 2: $\text{pix2pix}_{M \rightarrow C}$ has a generator G_A , which generates sCT from MR, and a discriminator D_A , which distinguishes between real CT and sCT. L_1 loss between MRCAT (pair of MR) and sCT is used as an auxiliary supervision.

translation, and MR motion correction [1]. Other potential generative models for unpaired image translation include Multimodal UNIT (MUNIT) [10], Disentangled Representation for Image-to-Image Translation++ (DRIT++) [17], Multi-Season GAN (MSGAN) [30], and StarGAN v2 [4].

We propose modifications to original pix2pix model for tasks $\text{CT} \rightarrow \text{MR}$ and $\text{MR} \rightarrow \text{CT}$ for situations where there is only unpaired CT and MR data. MR scans can be used to generate voxel-aligned (paired) Magnetic Resonance for Calculating ATtenuation (MRCAT) scans, which look somewhat like CT but are not very realistic and thus not suitable for many tasks (see Fig. 1). Our proposed models utilize the alignment information between MR and MRCAT as an auxiliary supervision and produce more realistic CT and MR translations.

2 Methods

We propose two pix2pix variants, $\text{pix2pix}_{M \rightarrow C}$ and $\text{pix2pix}_{C \rightarrow M}$, for tasks $\text{MR} \rightarrow \text{CT}$ and $\text{CT} \rightarrow \text{MR}$, respectively. These models are trained with unpaired CT and MR, and paired MR and MRCAT, which are used as auxiliary supervision to preserve anatomic alignment between input and translated images. We use U-Net-based [22] generators and PatchGAN discriminators as in [11].

$\text{pix2pix}_{M \rightarrow C}$ (MR \rightarrow CT): $\text{pix2pix}_{M \rightarrow C}$ consists of one generator G_A and an unconditional discriminator D_A (Fig. 2). The generator is trained to generate synthetic CT ($\text{sCT} = G_A(\text{MR})$) from real MR input, while the discriminator D_A is trained to classify between the sCT and real CT. $\text{pix2pix}_{M \rightarrow C}$ has an unconditional GAN objective, $\mathcal{L}_{GAN}(G_A, D_A)$, as the conditional GAN (cGAN) objective cannot be used due to lack of paired CT and MR. Following [8,11], D_A is trained to maximize this objective, while G_A is trained to maximize $\log(D_A(G_A(\text{MR})))$.

$$\mathcal{L}_{GAN}(G_A, D_A) = \mathbb{E}_{CT}[\log D_A(CT)] + \mathbb{E}_{MR}[\log(1 - D_A(G_A(MR)))] \quad (1)$$

In addition, G_A is trained to minimize an L_1 loss between MRCAT and the generated sCT, $\mathcal{L}_{L_1}(G_A)$. Note that we do not have ground truth CTs for the MRs, which is why we use MRCATs in the L_1 loss. The L_1 loss plays similar role as cGAN objective in original pix2pix [11] as it encourages the sCTs to

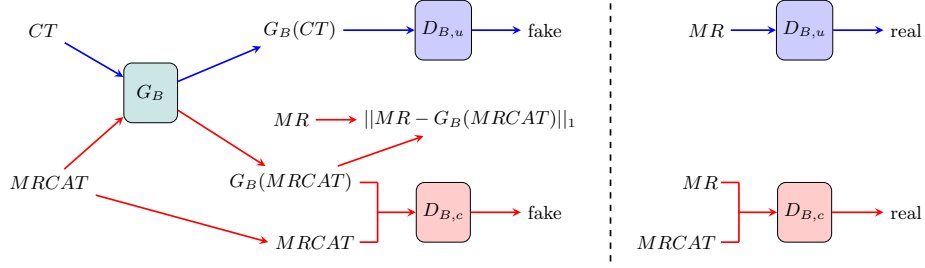


Fig. 3: $\text{pix2pix}_{C \rightarrow M}$ has a generator G_B , for producing sMR, and two discriminators, $D_{B,u}$ and $D_{B,c}$. $D_{B,c}$ is conditioned on the input MRCAT, and learns to classify between $G_B(\text{MRCAT})$ and real MR. $D_{B,u}$ distinguishes between $G_B(\text{CT})$ and real MR. \rightarrow : path for CT input. \rightarrow : path for MRCAT input.

be aligned with the input MRs. Our target distribution is the distribution of real CTs instead of MRCATs, which is why the MRCATs are only used as an auxiliary supervision.

$$\mathcal{L}_{L_1}(G_A) = \mathbb{E}_{\text{MRCAT}, \text{MR}}[\|\text{MRCAT} - G_A(\text{MR})\|_1] \quad (2)$$

The full training objective of $\text{pix2pix}_{M \rightarrow C}$ is

$$\mathcal{L}(G_A, D_A) = \mathcal{L}_{GAN}(G_A, D_A) + \lambda \mathcal{L}_{L_1}(G_A) \quad (3)$$

$\text{pix2pix}_{C \rightarrow M}$ (CT \rightarrow MR): $\text{pix2pix}_{C \rightarrow M}$ consists of one generator G_B and two discriminators $D_{B,u}$ and $D_{B,c}$. The generator takes either real CT, with probability of 0.5, or MRCAT as input during training, and it is trained to generate synthetic MR (sMR) images from both input modalities. The unconditional discriminator $D_{B,u}$ is trained to classify between the sMR generated from real CT, $G_B(\text{CT})$, and real MR. The conditional discriminator $D_{B,c}$ is conditioned on MRCAT, and is trained to classify between the synthetic MR generated from MRCAT, $G_B(\text{MRCAT})$, and real MR.

$\text{pix2pix}_{C \rightarrow M}$ has two GAN objectives: $\mathcal{L}_{GAN}(G_B, D_{B,u})$ and $\mathcal{L}_{cGAN}(G_B, D_{B,c})$. Following [8, 11], $D_{B,u}$ and $D_{B,c}$ are trained to maximize $\mathcal{L}_{GAN}(G_B, D_{B,u})$ and $\mathcal{L}_{cGAN}(G_B, D_{B,c})$, respectively, while G_B is trained to maximize $\log(D_{B,u}(G_B(\text{CT})))$ and $\log(D_{B,c}(\text{MRCAT}, G_B(\text{MRCAT})))$.

$$\mathcal{L}_{GAN}(G_B, D_{B,u}) = \mathbb{E}_{\text{MR}}[\log D_{B,u}(\text{MR})] + \mathbb{E}_{\text{CT}}[\log(1 - D_{B,u}(G_B(\text{CT})))] \quad (4)$$

$$\begin{aligned} \mathcal{L}_{cGAN}(G_B, D_{B,c}) = & \mathbb{E}_{\text{MRCAT}, \text{MR}}[\log D_{B,c}(\text{MRCAT}, \text{MR})] \\ & + \mathbb{E}_{\text{MRCAT}}[\log(1 - D_{B,c}(\text{MRCAT}, G_B(\text{MRCAT})))] \end{aligned} \quad (5)$$

In addition, G is trained to minimize the L_1 loss between MR and the sMR generated from MRCAT, $\mathcal{L}_{L_1}(G_B)$. Since we do not have paired CT and MR,

we cannot compute L_1 loss between $G_B(CT)$ and MR. While our primary goal is CT→MR translation, the introduction of MRCAT inputs allows us to use the alignment information between the MRCAT and MR pairs to encourage the generator to produce sMR that is aligned with the input.

$$\mathcal{L}_{L_1}(G_B) = \mathbb{E}_{MR, MRCAT}[\|MR - G_B(MRCAT)\|_1] \quad (6)$$

The full training objective of pix2pix $_{C \rightarrow M}$ is as follows

$$\mathcal{L}(G_B, D_{B,u}, D_{B,c}) = \mathcal{L}_{GAN}(G_B, D_{B,u}) + \mathcal{L}_{cGAN}(G_B, D_{B,c}) + \lambda \mathcal{L}_{L_1}(G_B) \quad (7)$$

Training details: We use random horizontal flip, random zoom (scale: 0.6–1.4) and random crop as data augmentations. In ablation experiments, we use down-sampled (by a factor of 4) images. We utilize the code [6,21] provided by the authors [11,32,25]. We use instance normalization, and a batch size of 8 for pix2pixHD, and batch size of 16 for the other models. All models are trained for 50 epochs, and 13K iterations per epoch. We use Adam optimizer with constant learning rate (LR) (0.0002) for the first 30 epochs and with linearly decaying LR from 0.0002 to zero over the last 20 epochs.

For pix2pix $_{M \rightarrow C}$ and pix2pix $_{C \rightarrow M}$, we use the vanilla GAN loss (the cross-entropy objective) like in original pix2pix [11] (Table 1). For pix2pix $_{C \rightarrow M}$ we use $\lambda = 100$, and discriminator receptive field (RF) size 70×70 in ablation (low resolution) experiments and 286×286 in our final model. For pix2pix $_{M \rightarrow C}$, we use $\lambda = 50$, and discriminator RF size 70×70 . Since CycleGAN with the default 70×70 discriminators fails, we use a stronger baseline CycleGAN with discriminator RF size 142×142 .

3 Experiments

Dataset: The dataset contains 51 pairs of Dixon-In-Phase (DIP) MR and MRCAT scans, and 220 unpaired CT scans of prostate cancer patients, treated with radiotherapy, from Turku University Hospital. The scans were randomly split into training and evaluation set. The number of training MR/MRCAT/CT scans is 41/41/179, and the number of evaluation MR/CT scans is 10/41.

Evaluation Metrics: We use Kernel Inception Distance (KID) [3] and Fréchet Inception Distance (FID) [9] between real and translated images as the evaluation metrics. They measure the distance between the distribution of the generated images and the target distribution of real images, and lower values indicate better performance. In addition, we use DICE coefficient between automatically segmented [14] structures (e.g. Body, Femurs, Prostate, etc.) of input and translated images to evaluate the anatomic alignment and quality of translations. For task MR→CT, we also compute the mean absolute HU intensity difference (HU-Dif) between mean HU value for each segmented ROI in real and translated CTs.

Table 1: Overview of the models. Paired data refers to MR and MRCAT pairs. CTs are unpaired with MRs/MRCATs.

Model	Generator	GAN mode	Training data	#CT	#MR	#MRCAT
CycleGAN	unet_512	lsgan	unpaired	179	41	0
pix2pixHD	global	lsgan	paired	0	41	41
pix2pix	unet_512	vanilla	paired	0	41	41
pix2pix $M \rightarrow C$ /pix2pix $C \rightarrow M$	unet_512	vanilla	unpaired & paired	179	41	41

Table 2: MR \rightarrow CT translation: Performance comparison.

Model	Training data			$FID_{CT,sCT}$	$KID_{CT,sCT}$	DICE	HU-Dif
	CT	MR	MRCAT				
CycleGAN	✓	✓		42.8	0.019	0.80±0.20	15.5
pix2pixHD		✓	✓	121.9	0.118	0.91±0.10	23.2
pix2pix		✓	✓	122.6	0.119	0.91±0.12	23.0
pix2pix $M \rightarrow C$	✓	✓	✓	34.3	0.009	0.88±0.14	16.1

3.1 Comparison with baselines

We compare our models, pix2pix $M \rightarrow C$ and pix2pix $C \rightarrow M$, with pix2pix [11] and pix2pixHD [25], and CycleGAN [32]. Table 1 provides the details of the models and training data.

MR \rightarrow CT: Table 2 shows that pix2pix $M \rightarrow C$ outperformed all other methods in terms of FID and KID, indicating that its translated images better resembled real CT. It had slightly worse DICE (standard deviation is much higher than the difference) compared to pix2pix and pix2pixHD, which can partly be explained by the fewer artifacts produced by these models. However, since pix2pix and pix2pixHD were trained using MRCAT as their target, their predictions had similar limitations as the MRCAT, e.g. clear quantization artifacts were present (see bones in Fig. 4). pix2pix and pix2pixHD had high FID and KID, primarily due to absence of the patient couch in the translated CT. CycleGAN translations had small misalignment with inputs and some moderate artifacts, lowering its DICE score. pix2pix $M \rightarrow C$ had some prominent artifacts, primarily in the bottom few slices, these might have been caused by the slight difference in the field-of-view of MR and CT datasets. pix2pix $M \rightarrow C$ and CycleGAN generated air cavities and hallucinated patient tables.

CT \rightarrow MR: pix2pix $C \rightarrow M$ had the best performance in terms of FID, KID and DICE, as shown in Table 3. pix2pix and pix2pixHD produced relatively good translations of the patient anatomy but due to their failure to ignore the couch (see Fig. 5), visible in CT, their FID and KID values were high. CycleGAN had the worst translations, with large artifacts in some parts of the body (see Fig. 5e), frequently causing large segmentation failures and leading to very low

DICE. $\text{pix2pix}_{C \rightarrow M}$ produced less artifacts and more realistic sMRs, however, some sMR slices had a small misalignment with inputs near the couch.

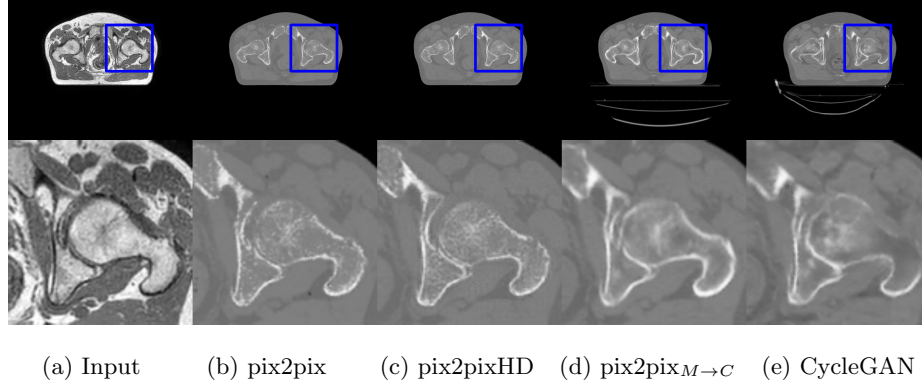


Fig. 4: sCTs produced by $\text{pix2pix}_{M \rightarrow C}$ and the baselines. First row: Slices from complete scans. Second row: cropped slices.

Table 3: CT \rightarrow MR translation: Performance comparison.

Model	Training data			$FID_{MR, sMR}$	$KID_{MR, sMR}$	DICE
	CT	MR	MRCAT			
CycleGAN	✓	✓		55.9	0.029	0.58 ± 0.29
pix2pix_{HD}		✓	✓	127.8	0.122	0.81 ± 0.17
pix2pix		✓	✓	90.8	0.086	0.81 ± 0.16
$\text{pix2pix}_{C \rightarrow M}$	✓	✓	✓	45.3	0.021	0.83 ± 0.15

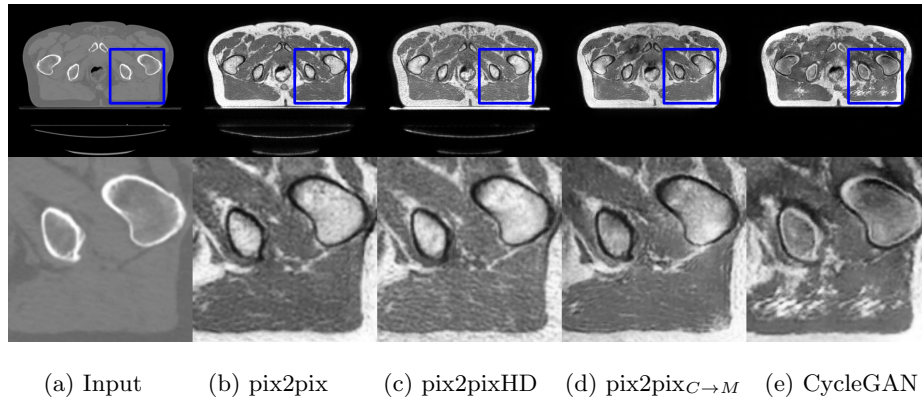


Fig. 5: sMRs generated by $\text{pix2pix}_{C \rightarrow M}$ and the baselines. First row: Slices from complete scans. Second row: cropped slices.

Table 4: Training objectives for $\text{pix2pix}_{M \rightarrow C}$ in low resolution. $\lambda = 50$.

Objective	Training data			$FID_{CT,sCT}$	$KID_{CT,sCT}$	DICE
	CT	MR	MRCAT			
L_1		✓	✓	147.4	0.146	0.72
GAN	✓	✓		67.3	0.032	0.23
GAN + λL_1	✓	✓	✓	39.4	0.014	0.73

Table 5: Training objectives for $\text{pix2pix}_{C \rightarrow M}$ in low resolution. $\lambda = 100$.

Objective	Training data			$FID_{MR,sMR}$	$KID_{MR,sMR}$	DICE
	CT	MR	MRCAT			
GAN	✓	✓		40.0	0.015	0.24
GAN+cGAN	✓	✓	✓	32.8	0.013	0.52
GAN+cGAN+ λL_1	✓	✓	✓	30.0	0.012	0.57

3.2 Ablation studies

$\text{pix2pix}_{M \rightarrow C}$ objective: When the training objective included both L_1 and GAN loss, the translations looked realistic and the performance of $\text{pix2pix}_{M \rightarrow C}$ was better in terms of FID, KID and DICE scores compared to the experiment with only L_1 objective or only GAN objective (Table 4). When only GAN objective was used, the generated sCTs had poor alignment with the input MRs.

$\text{pix2pix}_{C \rightarrow M}$ objective: When only CT inputs were used with a GAN objective (see \rightarrow path in Fig. 3), the generated sMR images were not well aligned with the inputs. The translations were better aligned when the cGAN objective was included, i.e. with a probability of 0.5 either CT or MRCAT input was used. Inclusion of the L_1 objective (between sMR generated from MRCAT and real MR) with GAN+cGAN produced the best results in terms of FID, KID and DICE (see Table 5).

4 Conclusion

Our results show that CT \rightarrow MR and MR \rightarrow CT translation with unpaired CT and MR, using the MR and MRCAT pairs as an auxiliary supervision, produces more realistic translated CT and MR images. This additional supervision reduces artifacts and improves alignment between the input and the translated images. The proposed $\text{pix2pix}_{M \rightarrow C}$ and $\text{pix2pix}_{C \rightarrow M}$, outperformed the baseline pix2pix , pix2pixHD and CycleGAN, in terms of FID and KID scores.

$\text{pix2pix}_{M \rightarrow C}$ and $\text{pix2pix}_{C \rightarrow M}$, like other GAN-based methods, may be useful in producing realistic-looking translated images for research purposes. Since these methods can hallucinate features in images [5], they require extensive validation of their image quality and fidelity before clinical use. It remains as task for future research to develop improved translation methods and design quantitative metrics which better capture the quality of translations.

References

1. Armanious, K., Jiang, C., Abdulatif, S., Küstner, T., Gatidis, S., Yang, B.: Unsupervised medical image translation using Cycle-MedGAN. In: 2019 27th European Signal Processing Conference (EUSIPCO). pp. 1–5. IEEE (2019)
2. Armanious, K., Jiang, C., Fischer, M., Küstner, T., Hepp, T., Nikolaou, K., Gatidis, S., Yang, B.: MedGAN: medical image translation using GANs. *Computerized Medical Imaging and Graphics* **79**, 101684 (2020)
3. Bińkowski, M., Sutherland, D.J., Arbel, M., Gretton, A.: Demystifying MMD GANs. arXiv preprint arXiv:1801.01401 (2018)
4. Choi, Y., Uh, Y., Yoo, J., Ha, J.W.: StarGAN v2: diverse image synthesis for multiple domains. In: Proceedings of the IEEE/CVF Conference on Computer Vision and Pattern Recognition. pp. 8188–8197 (2020)
5. Cohen, J.P., Luck, M., Honari, S.: Distribution matching losses can hallucinate features in medical image translation. In: International Conference on Medical Image Computing and Computer-Assisted Intervention. pp. 529–536. Springer (2018)
6. CycleGAN and pix2pix. <https://github.com/junyanz/pytorch-CycleGAN-and-pix2pix> (2021)
7. Emami, H., Dong, M., Nejad-Davarani, S.P., Glide-Hurst, C.K.: Generating synthetic CTs from magnetic resonance images using generative adversarial networks. *Medical Physics* **45**(8), 3627–3636 (2018)
8. Goodfellow, I.J., Pouget-Abadie, J., Mirza, M., Xu, B., Warde-Farley, D., Ozair, S., Courville, A., Bengio, Y.: Generative adversarial networks. arXiv preprint arXiv:1406.2661 (2014)
9. Heusel, M., Ramsauer, H., Unterthiner, T., Nessler, B., Hochreiter, S.: GANs trained by a two time-scale update rule converge to a local Nash equilibrium. arXiv preprint arXiv:1706.08500 (2017)
10. Huang, X., Liu, M.Y., Belongie, S., Kautz, J.: Multimodal unsupervised image-to-image translation. In: Proceedings of the European Conference on Computer Vision (ECCV). pp. 172–189 (2018)
11. Isola, P., Zhu, J.Y., Zhou, T., Efros, A.A.: Image-to-image translation with conditional adversarial networks. In: Proceedings of the IEEE Conference on Computer Vision and Pattern Recognition. pp. 1125–1134 (2017)
12. Jiang, J., Hu, Y.C., Tyagi, N., Rimner, A., Lee, N., Deasy, J.O., Berry, S., Veeraraghavan, H.: PSIGAN: joint probabilistic segmentation and image distribution matching for unpaired cross-modality adaptation-based MRI segmentation. *IEEE Transactions on Medical Imaging* **39**(12), 4071–4084 (2020)
13. Jin, C.B., Kim, H., Liu, M., Jung, W., Joo, S., Park, E., Ahn, Y.S., Han, I.H., Lee, J.I., Cui, X.: Deep CT to MR synthesis using paired and unpaired data. *Sensors* **19**(10), 2361 (2019)
14. Kiljunen, T., Akram, S., Niemelä, J., Löyttyniemi, E., Seppälä, J., Heikkilä, J., Vuolukka, K., Kääriäinen, O.S., Heikkilä, V.P., Lehtiö, K., Nikkinen, J., Gershkevitch, E., Borkvel, A., Adamson, M., Zolotuhhin, D., Kolk, K., Pang, E.P.P., Tuan, J.K.L., Master, Z., Chua, M.L.K., Joensuu, T., Kononen, J., Myllykangas, M., Riener, M., Mokka, M., Keyriläinen, J.: A deep learning-based automated CT segmentation of prostate cancer anatomy for radiation therapy planning—a retrospective multicenter study. *Diagnostics* **10**(11) (2020). <https://doi.org/10.3390/diagnostics10110959>
15. Kingma, D.P., Welling, M.: Auto-encoding variational Bayes. arXiv preprint arXiv:1312.6114 (2013)

16. Larsen, A.B.L., Sønderby, S.K., Larochelle, H., Winther, O.: Autoencoding beyond pixels using a learned similarity metric. In: International Conference on Machine Learning. pp. 1558–1566. PMLR (2016)
17. Lee, H.Y., Tseng, H.Y., Mao, Q., Huang, J.B., Lu, Y.D., Singh, M., Yang, M.H.: DRIT++: diverse image-to-image translation via disentangled representations. International Journal of Computer Vision **128**(10), 2402–2417 (2020)
18. Liu, M.Y., Breuel, T., Kautz, J.: Unsupervised image-to-image translation networks. arXiv preprint arXiv:1703.00848 (2017)
19. Nie, D., Trullo, R., Lian, J., Petitjean, C., Ruan, S., Wang, Q., Shen, D.: Medical image synthesis with context-aware generative adversarial networks. In: International Conference on Medical Image Computing and Computer-Assisted Intervention. pp. 417–425. Springer (2017)
20. Peng, Y., Chen, S., Qin, A., Chen, M., Gao, X., Liu, Y., Miao, J., Gu, H., Zhao, C., Deng, X., et al.: Magnetic resonance-based synthetic computed tomography images generated using generative adversarial networks for nasopharyngeal carcinoma radiotherapy treatment planning. Radiotherapy and Oncology **150**, 217–224 (2020)
21. pix2pixHD. <https://github.com/NVIDIA/pix2pixHD> (2021)
22. Ronneberger, O., Fischer, P., Brox, T.: U-net: convolutional networks for biomedical image segmentation. In: International Conference on Medical Image Computing and Computer-Assisted Intervention. pp. 234–241. Springer (2015)
23. Sandfort, V., Yan, K., Pickhardt, P.J., Summers, R.M.: Data augmentation using generative adversarial networks (CycleGAN) to improve generalizability in CT segmentation tasks. Scientific Reports **9**(1), 1–9 (2019)
24. Tanner, C., Ozdemir, F., Profanter, R., Vishnevsky, V., Konukoglu, E., Goksel, O.: Generative adversarial networks for MR-CT deformable image registration. arXiv preprint arXiv:1807.07349 (2018)
25. Wang, T.C., Liu, M.Y., Zhu, J.Y., Tao, A., Kautz, J., Catanzaro, B.: High-resolution image synthesis and semantic manipulation with conditional GANs. In: Proceedings of the IEEE Conference on Computer Vision and Pattern Recognition. pp. 8798–8807 (2018)
26. Welander, P., Karlsson, S., Eklund, A.: Generative adversarial networks for image-to-image translation on multi-contrast MR images-a comparison of CycleGAN and UNIT. arXiv preprint arXiv:1806.07777 (2018)
27. Wolterink, J.M., Dinkla, A.M., Savenije, M.H., Seevinck, P.R., van den Berg, C.A., Išgum, I.: Deep MR to CT synthesis using unpaired data. In: International Workshop on Simulation and Synthesis in Medical Imaging. pp. 14–23. Springer (2017)
28. Wolterink, J.M., Leiner, T., Viergever, M.A., Išgum, I.: Generative adversarial networks for noise reduction in low-dose CT. IEEE Transactions on Medical Imaging **36**(12), 2536–2545 (2017)
29. Yi, X., Walia, E., Babyn, P.: Generative adversarial network in medical imaging: a review. Medical Image Analysis **58**, 101552 (2019)
30. Zhang, F., Wang, C.: MSGAN: generative adversarial networks for image seasonal style transfer. IEEE Access **8**, 104830–104840 (2020)
31. Zhang, Z., Yang, L., Zheng, Y.: Translating and segmenting multimodal medical volumes with cycle- and shape-consistency generative adversarial network. In: CVPR (2018), <http://arxiv.org/abs/1802.09655>
32. Zhu, J.Y., Park, T., Isola, P., Efros, A.A.: Unpaired image-to-image translation using cycle-consistent adversarial networks. In: Proceedings of the IEEE International Conference on Computer Vision. pp. 2223–2232 (2017)